Article

Antarctic Peninsula glaciation patterns set by landscape evolution and dynamic topography

Matthew Fox [1] ✉, Anna Clinger[2,3], Adam G. G. Smith [1,4], Kurt Cuffey [2], David Shuster[2,3] & Frederic Herman [5]

The dimensions of past ice sheets provide a record of palaeoclimate but depend on underlying topography, which evolves over geological timescales by tectonic uplift and erosional downcutting. Erosion during the Pleistocene epoch (2,580 to 11.650 thousand years ago) reduced glacier extent in some locations even as climate cooled, but whether other non-climatic influences impacted the glacial–geological record is poorly known. The Antarctic Peninsula provides an opportunity to examine this issue because of its long glacial history and preservation of remnants of a low-relief pre-glacial land surface. Here we reconstructed both palaeo-surface topography and long-wavelength variations of surface uplift for the Antarctic Peninsula by using inverse analysis that assimilates local topographic remnants with the branching structures of entire modern drainage networks. We found that the Antarctic Peninsula rose tectonically by up to 1.5 km due to dynamical support from the mantle. Glaciological models using the current climate and our palaeotopography show greatly reduced ice extent in the northern Antarctic Peninsula compared with modern, indicating that the onset of glaciation identified at offshore sites reflects tectonic uplift of the topography rather than climatic cooling. In the southern Antarctic Peninsula, however, we suggest the low-relief pre-glacial landscape supported a considerably greater ice volume than the modern mountainous topography, illustrating the influence of erosional sculpting on glaciation patterns.

Evolving topography in glaciated regions not only complicates interpretations of past climates but also exerts a fundamental influence on past ice-sheet dynamics and creates the framework for present ice-sheet behaviour[1–5]. Today, the Antarctic Peninsula (AP) is rapidly warming and contributing to sea-level rise as its glaciers retreat from grounding lines located in deeply incised fjords[6]. These fjords dissect a gently undulating topographic plateau that constitutes the spine of the AP (Fig. 1c)[7]. We can leverage this topography to create an estimate of the pre-glacial topography, facilitating more-realistic assessment of the climatic conditions required to initiate ice-sheet growth on the AP.

Alpine glaciation was initiated on the AP by 37–34 Ma (ref. 2), and the extent of glaciation has been closely linked to Cenozoic climate change. The start of AP glaciation occurred when global temperatures were 4 °C higher than today[8–10] and might have been a response to the

[1]Department of Earth Sciences, University College London, London, UK. [2]Department of Earth and Planetary Science, University of California, Berkeley, CA, USA. [3]Berkeley Geochronology Center, Berkeley, CA, USA. [4]Department of Earth and Planetary Science Birkbeck, University of London, London, UK. [5]Institute of Earth Surface Dynamics, University of Lausanne, Lausanne, Switzerland. ✉e-mail: m.fox@ucl.ac.uk
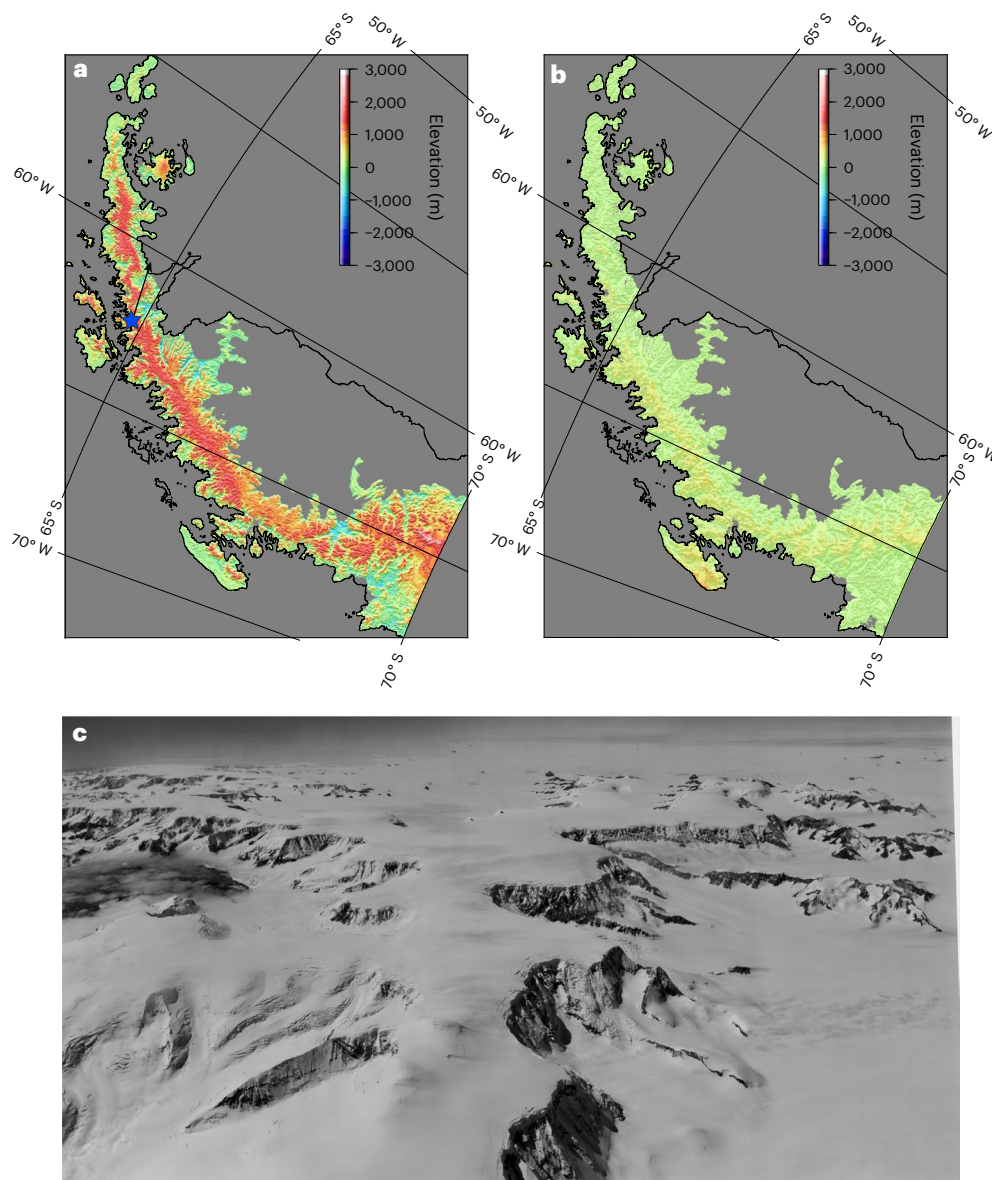
Fig. 1 | Topographic change along the AP. a, The topography of the AP today shows a low-relief, high-elevation spine dissected by glacial valleys. The elevation of the spine is slightly higher in the north than in the south. The greatest ridge-to-valley relief is approximately 3,000 m where the spine is high, and the valleys are deeply incised. **b,** The pre-glacial, fluvial landscape as predicted from our inversion. Elevations along the length of the AP are lower, and the greatest relief is approximately 1,000 m. The over-deepened glacial valleys have been filled with graded river profiles following Flint's Law[17]. The position of the base level is held constant; however, there is sufficient flexibility in the model to account for errors introduced by changes in the position of the base level. **c,** Low-relief, high-elevation surface of the AP looking towards the northwest. The location and direction of the view are indicated in panel **a** by the blue star and arrow. Panorama in **c** made from trimetrogon aerial photography collected by the US Navy on 27 December 1968, flightline 2152, frames 364R to 368R.

development of the Antarctic Circumpolar Current during the tectonic opening of the Drake Passage[11,12] or a decline in p_{CO_2} (ref. 8). Progressive cooling potentially caused expansion of ice and a permanent, poly-thermal ice sheet was established by 9 million years ago (Ma) (refs. 2,9).

The early Antarctic ice sheets, in general, were thinner and more dynamic than those of today, and they fluctuated on Milankovitch frequencies[13]. It has been assumed that >2 km high topography of the AP may have acted as a focus for ice-sheet nucleation in response to orographically forced precipitation in climates that were warmer and wetter than at present[14]. Antarctic topography, however, has been reconstructed only at a continental scale[15,16] not at the detail or physical basis required for catchment-scale glacial modelling across the AP.

In this Article, we exploit remnants of the low-relief fluvial networks of the northern part of the AP to reconstruct a fluvial landscape that obeys geomorphic scaling laws (Methods)[17,18]. This is in contrast to

previous approaches for topographic reconstruction, which generate smooth topography by interpolating a surface through topographic highs and ultimately lack the clear nucleation sites and topographic hypsometry necessary for mountain glaciation[15,16,19]. As a result, our topographic reconstruction provides a physically plausible topographic boundary condition. The requirement that the topography is realistic also provides independent constraints on tectonic uplift and landscape evolution. Ice-sheet simulations on a realistic palaeotopography illustrate quantitatively how topography affects glacial extent even with invariant climatic conditions.

Topographic data and fluvial reconstruction

The topographic data we used for this analysis are from the 100-m-resolution digital elevation model (DEM) of ref. 20, which captures the current topography of the AP under the ice. This model
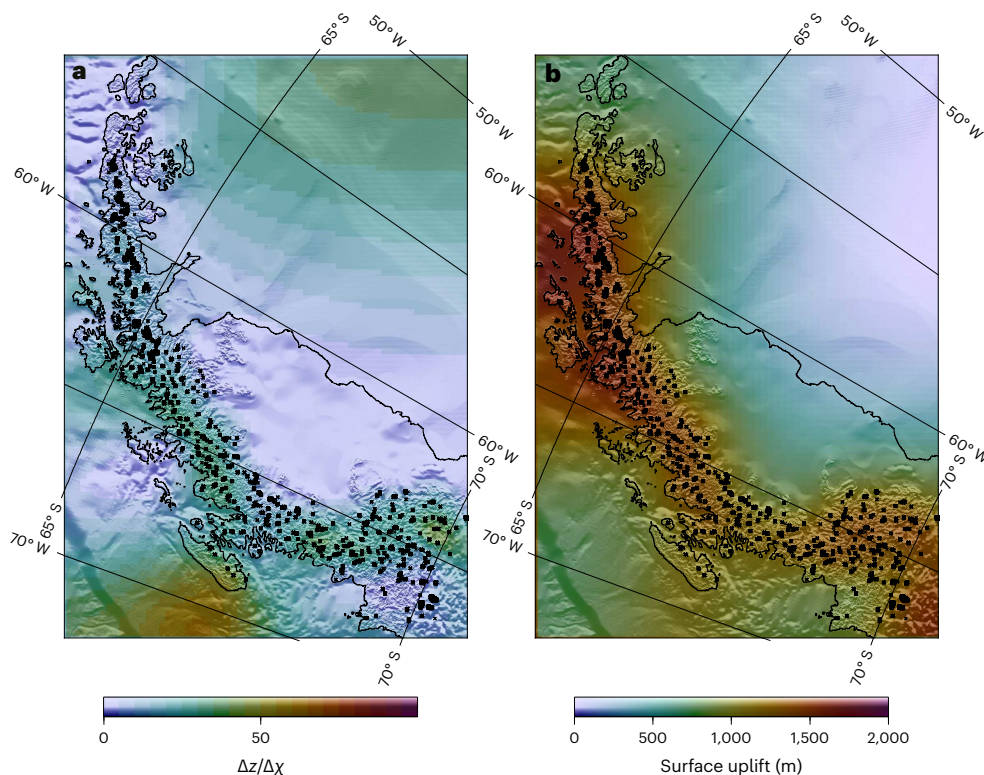
Fig. 2 | The elevations of the remnant surfaces are a function of parameters controlling the relief on the fluvial pre-glacial landscape and the more recent surface uplift. These parameters can be obtained through linear inversion of the stream power model using the remnant elevations as data points (black crosses). **a**, The normalized rock uplift rate (dz/dχ, or u^*) describes the steepness of a river accounting for changes in upstream drainage area. This information is preserved by local variations in elevation and the branching river network. **b**, The surface uplift describes the additional amount of elevation difference between the modern topography and the elevations obtained by integrating slopes along the river profiles. Our inversion minimizes elevation misfit and the spatial smoothness of the u^* ($\alpha W_u u^*$) and s.u. ($\lambda W_{s.u.}$ s.u.) parameter maps. The contribution of the smoothness constraints to the total misfit is weighted by $\alpha = 10^2$ and $\lambda = 10^1$. See Methods for information on the parameters.

has been constructed only where there is ice, and we use the BEDMAP 2 bedrock model[21] for areas not covered by the 100 m DEM (Fig. 1a). The AP includes low-slope topographic surfaces at high elevations along its length. This surface appears to be dissected by deep glacial valleys and glacial cirques (Fig. 1c). The alternative explanation, that low-relief surfaces formed in response to glacial bevelling of previous high-relief topography, is negated by the available thermochronometry, which indicates relatively recent (<15 Ma) development of the deep glacial valleys and slow erosion rates across the low-slope surfaces[22]. Ridge-to-sea-level relief along the length of the peninsula is relatively uniform at approximately 2 km (Fig. 1a). In general, the western side of the AP is steeper with a greater degree of glacial dissection than the eastern side. Before we reconstructed the topography, we first calculated flexural rebound associated with removal of the ice using an effective elastic thickness of 35 km, Poisson's ratio of 0.25, a crustal density of 2,700 kg m^{-3}, mantle density of 3,200 kg m^{-3}, ice density of 920 kg m^{-3} and a Young's modulus of 7.0×10^{10} N m^{-2}. This rebounded topography provided the data points for our inverse scheme, outlined in the following.

We extracted the drainage network using the Terraflow function in GRASS (Geographic Resources Analysis Support System)[23], where all depressions are filled to account for overdeepenings and errors in the DEM. However, this is simply to calculate the flow routing: the topographic reconstructions interpolated over the overdeepenings with sloping river profiles. Once the drainage network was obtained, we calculated values of normalized response time, or χ, for all points in the landscape with an upstream drainage area greater than 0.5 km^2; χ is the time that information takes to propagate upstream from the base level normalized to a uniform erodibility[24,25]. If knickpoints

arrive at the drainage divide at different times, erosion rates will differ and the divide will migrate. For our purposes, we used the analytical stream power model, which relates χ to elevation. To down-sample the data, once χ had been calculated using the high-resolution DEM, we randomly selected 15% of the dataset. Reducing the size of the dataset is important for the following inversion. This random process ensures that high χ values are probably found close to low χ values, improving resolution, and prevents selection biases.

Our inversion approach is based on the steady-state stream power model[18,26]. This states that the elevation of a node within the low-relief surface is equal to the integral of normalized rock uplift rate, u^*, along the profile of the river from the base level to the χ value (Methods),

$$z(x) = \int_0^{\chi(x)} \left(\frac{u(\chi')}{KA_0^m} \right)^{\frac{1}{n}} d\chi' \tag{1}$$

and $u^* = (u/KA_0^m)^{1/n}$ (ref. 24), where u is the rock uplift rate (with respect to base level) and K, A_0, n and m are constants within the stream power incision model (Methods). In this way, u^* represents a scaled rock uplift rate. If the rock uplift rate increases, knickpoints will propagate upstream, but the landscape above the knickpoints will preserve the previous uplift rate conditions. Similarly, if glacial erosion has been minimal across the low-relief landscape of the AP but intense within glacial valleys, the low-relief landscape can be used to infer the previous normalized rock uplift conditions. These conditions can then be extrapolated across the incised, rebounded topography and used to reconstruct a fluvial landscape. To do this, we state that the elevation is a combination of steady-state palaeotopography plus
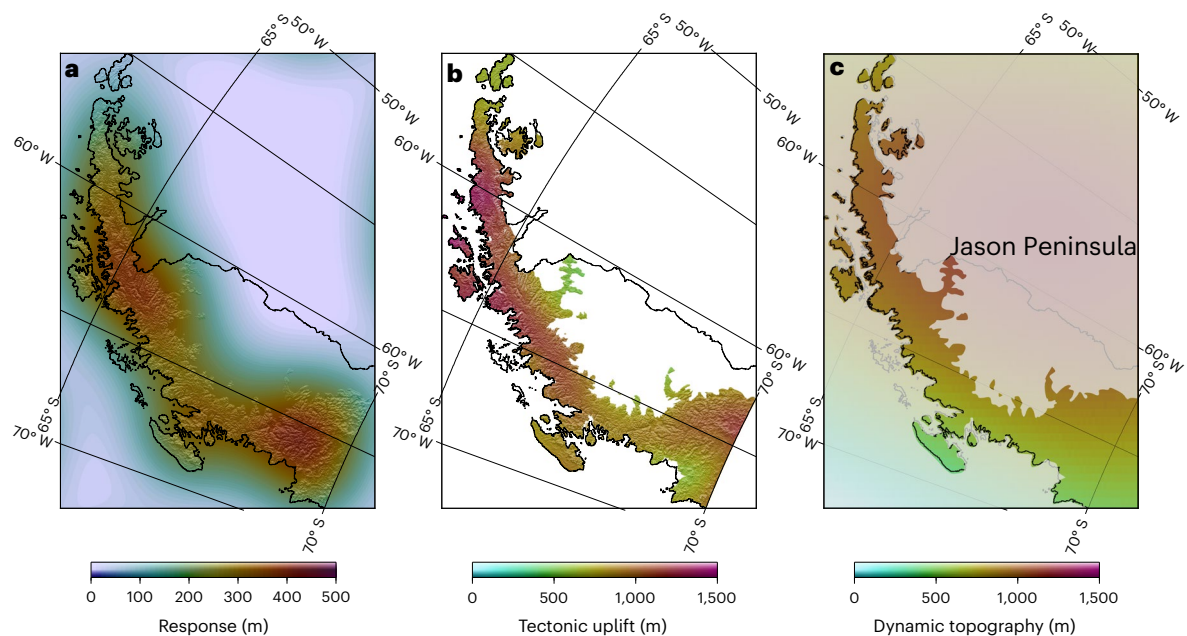
Fig. 3 | Surface uplift of the spine of the Antarctic Peninsula is a combination of primary tectonic uplift and isostatic response. a, The isostatic response is calculated by subtracting the modern ice-free, rebounded topography from the uplifted pre-glacial topography to calculate the amount of incision. This incision is a negative load, and the deflection of an elastic plate due to this load is calculated assuming an elastic plate of 35 km. **b**, The surface uplift, extracted from the spine of the AP, minus the valley incision rebound provides the primary tectonic uplift. Highest values are approximately 1,400 m around Anvers Island. Tectonic uplift decreases towards the north and south and is lowest close to Adelaide Island at around 700 m. An area of high uplift is observed on the east side of the AP. This is called Jason Peninsula, and we expect that this area of flat topography is actually uplifted continental shelf and does not represent part of a palaeo-surface. **c**, Independently constrained dynamic topography across the AP shows a very similar pattern to the tectonic uplift, with highest values close to Anvers Island, decreasing towards the north and south. The similarity in the magnitude and pattern of our inferred tectonic uplift and the dynamic topography indicates that dynamic topography is responsible for the uplift of the AP.

an additional component of surface uplift (measured with respect to base level). This surface uplift (s.u.) varies spatially but, based on the topography, must be a long-wavelength function. We discretize space into pixels of constant u^* and s.u. values. The resulting discrete equations of elevation as a function of along-channel normalized rock uplift and local s.u. are arranged in matrix–vector form and solved with smoothness constraints[27] (Methods). This linear inverse method is preferable to approaches to build fluvial landscapes that require known rock uplift functions[28] or nonlinear methods[3] because it solves for unknown rock uplift and surface uplift functions.

It is important to note that low-relief, high-elevation topography can be developed in fluvial landscapes through changes in rock uplift rate or drainage capture[29]. In turn, a low-relief, high-elevation landscape with deeply incised fluvial canyons may have existed before glaciation. This is unlikely because detrital thermochronometry reveals that valley incision occurred at about 15 Ma, after the initiation of glaciation in the region[22], and generally coincided with the arrival times of the spreading ridge at different latitudes. Therefore, the palaeotopography we resolve probably existed before 15 Ma and was later uplifted and dissected.

We selected an inversion result that represents a compromise between fit to the data and model smoothness to reconstruct the topography (Fig. 2). The model shows short-wavelength variations in u^* that lead to the steeper western side of the AP and long-wavelength variations in s.u. that are consistent with the relatively uniform elevation of the low-relief landscape. The variability in u^* probably reflects local variations in lithology, which are unknown below the ice, and potentially geomorphic noise (artefacts in the DEM and flow-routing algorithms, drainage divide migration or modifications of the low-relief topography by glacial erosion). The long-wavelength uplift s.u. contains two components: (1) the primary tectonic uplift; (2) the secondary isostatic response to glacial incision. Therefore, we subtracted the rebounded topography from the predicted and uplifted palaeo-topography to calculate the change in topographic volume. Note this topographic volume is not equivalent to total sediment production of the AP (for a full discussion, see the Supplementary Information Section 3). The topographic volume was converted to a mass, which was used to calculate the flexural response to this mass change using an effective elastic thickness of 35 km and a Poisson's ratio of 0.25. Removing this secondary isostatic component of s.u., which can reach values of 500 m, provides the primary uplift. The overall pattern of primary uplift is approximately radial, displaying key similarities to the estimated dynamic topography inferred from a global tectonic model (Fig. 3c)[30], with maximum values of 1.4 km close to 65° S that decay to the north (Fig. 3b). We note that dynamic topography is difficult to constrain and alternative models exist; however, the comparison is encouraging. Therefore, the high elevations of the AP can be explained as a combination of isostatic response to erosion and dynamic topography. Here dynamic topography may be the result of opening of a slab window behind subducting oceanic ridge lithosphere[31]. This would also lead to a general younging of surface uplift towards the north[32,33].

Ice-sheet reconstructions

To reveal the sensitivity of the ice sheets across the Antarctic Peninsula, we used a simplified ice-sheet model[34] based on the shallow-ice approximation (SIA). This simplified model is sufficient to illustrate how changes in topography strongly influence ice-sheet extents. In this model, the accumulation rate is set to 2 m yr^{-1} (ref. 35), the equilibrium line altitude (ELA) is set to 500 m and the mass-balance gradient is set to 0.04 m^{-1}. This is higher than the estimated ELA (up to 400 m (ref. 36)) because with a lower ELA, our glaciers extend out into the surrounding ocean and the SIA is not suited for buoyant glaciers. Other parameters used in the ice model are given in ref. 34. These parameters result in an ice sheet that is roughly consistent with the modern ice-sheet
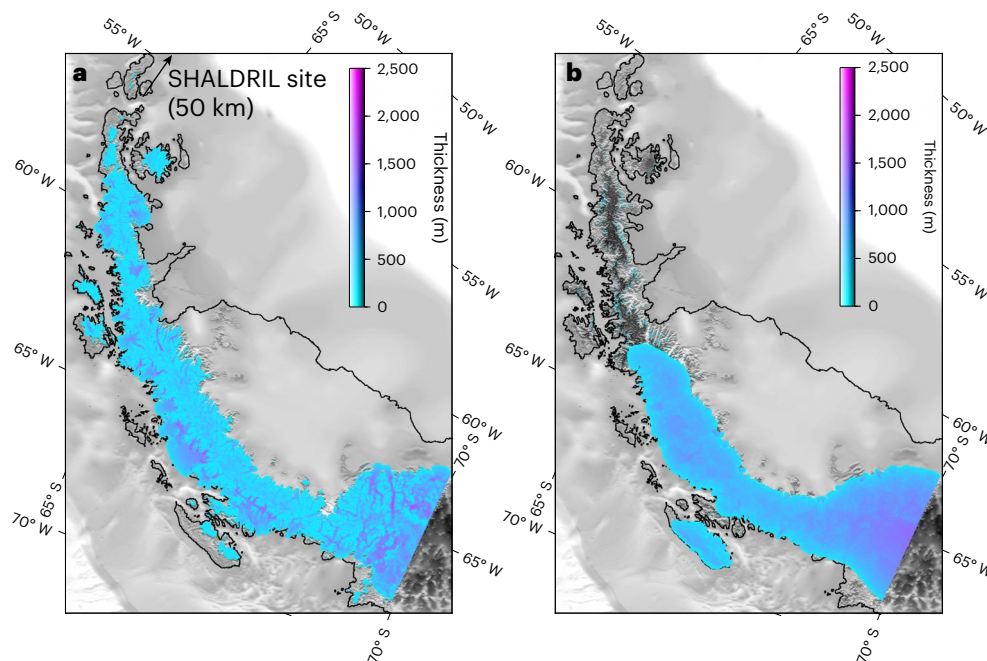
Fig. 4 | Ice-sheet simulations on the two topographies highlights topographic control on glaciation. a, A simple SIA model reproduces the general pattern of modern glaciation on the modern topography. **b**, The same model parameters produce a very different pattern of glaciation on the pre-glacial topography. Importantly, it appears that the pre-glacial landscape can support more ice south of approximately 66° S but less ice to the north of this location, for a simplified modern climate. This highlights how uplift and erosion control the amount of ice topography can support. The SHALDRIL site is just to the northeast of our study area.

extents using the modern topography (Fig. 4a). If we use the same climatic parameters for the pre-glacial topography, we see that the ice sheet is thicker but the extent of the ice sheet is much smaller (Fig. 4b). In fact, the volume of ice north of 70° S that is predicted on the pre-glacial topography is 4.4×10^4 km^3, but on the modern topography it is 4.0×10^4 km^3. However, considering northern and southern regions separately, divided at 66° S, the changes in ice volume are important and differ by region: the volume of ice increases in the north from 1.3×10^4 km^3 in the pre-glacial landscape to 1.8×10^4 km^3 in the modern topography but decreases in the south from 3.1×10^4 km^3 to 2.2×10^4 km^3. The uplift and dissection of the AP has enhanced ice-sheet growth in the north while inhibiting it in the south.

Our findings have some important implications for the onset and advance of glaciation on the AP as interpreted from the SHALDRIL cores[10]. The onset of mountain glaciation on the AP is inferred as early as 35.9 Ma, but the provenance of glacial dropstones is proposed to be either from the James Ross Island, proximal to the SHALDRIL sites, or from further south on the AP[10]. Our findings provide evidence that the latter is more likely. Furthermore, the timeline for advance of glaciation on the AP, although admittedly limited by the depositional ages of sampled sedimentary core, matches our timeline for relief production on the AP and the inferred advance of ice sheets to their present extent. An increase from minor glacial influence in offshore sediment north of the AP at ~24 Ma to the advance of an ice sheet in the northern part of the AP by ~12 Ma (ref. 10) had previously been suggested to be caused by climate change in the middle Miocene. However, relief production from 15 Ma (ref. 22) and the uplift of the pre-glacial topography to the modern topography could also explain glacial advance in the vicinity of the SHALDRIL site on the same timescale.

Implications for glaciation on evolving topography

It is essential to account for topographic evolution when interpreting ice-sheet extent in terms of climate change, and few have accounted for this with realistic topography[37,38]. The iconic topography of the

Antarctic Peninsula, with its low-relief, high-elevation spine, provides a unique record of transience that can be exploited to resolve surface uplift and normalized rock uplift rate. In this Article, we show that high elevations are the result of primary tectonic uplift and isostatic response to large-scale dissection. The primary tectonic uplift can be explained in terms of dynamic topography. Under a modern (or interglacial) climate, the restored pre-glacial topography can support a similar volume of ice, but the spatial pattern of glaciation is very different from the modern pattern. This highlights the influence of dynamic topography on glaciation, as has been shown across the East Antarctic Ice Sheet over the past 3 million years for the case of ice-sheet retreat and stability[39]. Transition between the pre-glacial topography and the uplifted and dissected landscape explains the apparent advance of ice sheets across the north of the peninsula, without invoking climatic changes. Glacial erosion has dissected the landscape, and the associated isostatic uplift increases surface slopes and forms deep valleys with elevations below the ELA. Ultimately, glacial erosion reduces the amount of ice the landscape can support. Similar impacts of topographic changes are likely across other glaciated landscapes and should be evaluated when estimating past climatic conditions from glacial deposits.

Online content

Any methods, additional references, Nature Portfolio reporting summaries, source data, extended data, supplementary information, acknowledgements, peer review information; details of author contributions and competing interests; and statements of data and code availability are available at https://doi.org/10.1038/s41561-023-01336-7.

References

1. Kaplan, M. R., Hein, A. S., Hubbard, A. & Lax, S. M. Can glacial erosion limit the extent of glaciation? *Geomorphology* **103**, 172–179 (2009).
2. Anderson, J. B. et al. Progressive Cenozoic cooling and the demise of Antarctica's last refugium. *Proc. Natl Acad. Sci. USA* **108**, 11356–11360 (2011).

3. Sternai, P. et al. Pre-glacial topography of the European Alps. *Geology* **40**, 1067–1070 (2012).

4. Clague, J. J. et al. Pliocene and early Pleistocene glaciation and landscape evolution on the Patagonian Steppe, Santa Cruz province, Argentina. *Quat. Sci. Rev.* **227**, 105992 (2020).

5. Anderson, R. S., Dühnforth, M., Colgan, W. & Anderson, L. Far-flung moraines: exploring the feedback of glacial erosion on the evolution of glacier length. *Geomorphology* **179**, 269–285 (2012).

6. Joughin, I. & Alley, R. B. Stability of the West Antarctic Ice Sheet in a warming world. *Nat. Geosci.* **4**, 506–513 (2011).

7. Nichols, R.L. Geomorphology of Antarctica. In *Antarctic Soils and Soil Forming Processes*, J.C.F. Tedrow (Ed.). (1966) https://doi.org/10.1029/AR008p0001

8. DeConto, R. M. & Pollard, D. Rapid Cenozoic glaciation of Antarctica induced by declining atmospheric CO_2. *Nature* **421**, 245–249 (2003).

9. Smellie, J. L., Haywood, A. M., Hillenbrand, C.-D., Lunt, D. J. & Valdes, P. J. Nature of the Antarctic Peninsula Ice Sheet during the Pliocene: geological evidence and modelling results compared. *Earth Sci. Rev.* **94**, 79–94 (2009).

10. Wellner, J. S., Anderson, J. B., Ehrmann, W., Weaver, F. M., Kirshner, A., Livsey, D. and Simms, A. R. History of an Evolving Ice Sheet as Recorded in SHALDRIL Cores from the Northwestern Weddell Sea, Antarctica. In *Tectonic, Climatic, and Cryospheric Evolution of the Antarctic Peninsula* (eds J.B. Anderson and J.S. Wellner). (2011) https://doi.org/10.1029/2010SP001047

11. Mayewski, P. A. et al. State of the Antarctic and Southern Ocean climate system. *Rev. Geophys.* **47**, RG1003 (2009).

12. Sauermilch, I. et al. Gateway-driven weakening of ocean gyres leads to Southern Ocean cooling. *Nat. Commun.* **12**, 6465 (2021).

13. Naish, T. et al. Obliquity-paced Pliocene West Antarctic Ice Sheet oscillations. *Nature* **458**, 322–328 (2009).

14. Siegert, M. J. Antarctic subglacial topography and ice-sheet evolution. *Earth Surf. Process. Landf.* **33**, 646–660 (2008).

15. Wilson, D. S. et al. Antarctic topography at the Eocene–Oligocene boundary. *Palaeogeogr. Palaeoclimatol. Palaeoecol.* **335–336**, 24–34 (2012).

16. Paxman, G. J. G. et al. Reconstructions of Antarctic topography since the Eocene–Oligocene boundary. *Palaeogeogr. Palaeoclimatol. Palaeoecol.* **535**, 109346 (2019).

17. Flint, J. J. Stream gradient as a function of order, magnitude, and discharge. *Water Resour. Res.* **10**, 969–973 (1974).

18. Howard, A. D. A detachment-limited model of drainage basin evolution. *Water Resour. Res.* **30**, 2261–2285 (1994).

19. Pedersen, V. K. & Egholm, D. L. Glaciations in response to climate variations preconditioned by evolving topography. *Nature* **493**, 206–210 (2013).

20. Huss, M. & Farinotti, D. A high-resolution bedrock map for the Antarctic Peninsula. *Cryosphere* **8**, 1261–1273 (2014).

21. Fretwell, P. et al. Bedmap2: improved ice bed, surface and thickness datasets for Antarctica. *Cryosphere* **7**, 375–393 (2013).

22. Clinger, A. E., Fox, M., Balco, G., Cuffey, K. & Shuster, D. L. Detrital thermochronometry reveals that the topography along the Antarctic Peninsula is not a Pleistocene landscape. *J. Geophys. Res. Earth Surf.* **125**, e2019JF005447 (2020).

23. Arge, L. et al. Efficient flow computation on massive grid terrain datasets. *GeoInformatica* **7**, 283–313 (2003).

24. Perron, J. T. & Royden, L. An integral approach to bedrock river profile analysis. *Earth Surf. Process. Landf.* **38**, 570–576 (2013).

25. Willett, S. D., McCoy, S. W., Perron, J. T., Goren, L. & Chen, C.-Y. Dynamic reorganization of river basins. *Science* **343**, 1248765 (2014).

26. Fox, M. & Carter, A. Heated topics in thermochronology and paths towards resolution. *Geosciences* **10**, 375 (2020).

27. Smith, A. G. G., Fox, M., Schwanghart, W. & Carter, A. Comparing methods for calculating channel steepness index. *Earth Sci. Rev.* **227**, 103970 (2022).

28. Gołędowski, B., Egholm, D. L., Nielsen, S. B., Clausen, O. R. & McGregor, E. D. Cenozoic erosion and flexural isostasy of Scandinavia. *J. Geodyn.* **70**, 49–57 (2013).

29. Whipple, K. X., DiBiase, R. A., Ouimet, W. B. & Forte, A. M. Preservation or piracy: diagnosing low-relief, high-elevation surface formation mechanisms. *Geology* **45**, 91–94 (2017).

30. Hoggard, M. J., White, N. & Al-Attar, D. Global dynamic topography observations reveal limited influence of large-scale mantle flow. *Nat. Geosci.* **9**, 456–463 (2016).

31. Guenthner, W. R., Barbeau, D. L., Reiners, P. W. & Thomson, S. N. Slab window migration and terrane accretion preserved by low-temperature thermochronology of a magmatic arc, northern Antarctic Peninsula. *Geochem. Geophys. Geosyst.* https://doi.org/10.1029/2009GC002765 (2010).

32. Larter, R. D. & Barker, P. F. Effects of ridge crest–trench interaction on Antarctic–Phoenix spreading: forces on a young subducting plate. *J. Geophys. Res.* **96**, 19583–19607 (1991).

33. Clinger, A., Fox, M., Balco, G., Cuffey, K. & Shuster, D. Tectonic controls on the timing of fjord incision at the Antarctic Peninsula. *Earth Planet. Sci. Lett.* **585**, 117528 (2022).

34. Višnjević, V., Herman, F. & Prasicek, G. Climatic patterns over the European Alps during the LGM derived from inversion of the paleo-ice extent. *Earth Planet. Sci. Lett.* **538**, 116185 (2020).

35. Lenaerts, J. T. M., Van Den Broeke, M. R., Van De Berg, W. J., Van Meijgaard, E. & Kuipers Munneke, P. A new, high-resolution surface mass balance map of Antarctica (1979–2010) based on regional atmospheric climate modeling: SMB ANTARCTICA. *Geophys. Res. Lett.* https://doi.org/10.1029/2011GL050713 (2012).

36. Ingólfsson, Ó., Hjort, C. & Humlum, O. Glacial and climate history of the Antarctic Peninsula since the Last Glacial Maximum. *Arct. Antarct. Alp. Res.* **35**, 175–186 (2003).

37. Gasson, E., DeConto, R. & Pollard, D. Antarctic bedrock topography uncertainty and ice sheet stability. *Geophys. Res. Lett.* **42**, 5372–5377 (2015).

38. Paxman, G. J. G., Gasson, E. G. W., Jamieson, S. S. R., Bentley, M. J. & Ferraccioli, F. Long-term increase in Antarctic Ice Sheet vulnerability driven by bed topography evolution. *Geophys. Res. Lett.* **47**, e2020GL090003 (2020).

39. Austermann, J. et al. The impact of dynamic topography change on Antarctic Ice Sheet stability during the mid-Pliocene warm period. *Geology* **43**, 927–930 (2015).

Methods

To process the information constraining landscape evolution, we use the normalized analytical, steady-state stream power model,

$$z(x) = z(x_b) + \left(\frac{U}{KA_0^m}\right)^{\frac{1}{n}} \chi \qquad (2)$$

where z is the elevation, x is the along-stream distance from base level, x_b is the base level, U is the rock uplift rate, K is the erodibility, and m and n are the area and slope exponents of the detachment-limited stream power model[18]; $(U/A_0^m K)^{1/n}$ is the normalized rock uplift rate, which is termed u^*. Equation 2 relies on the χ transformation[24], a transformation of the horizontal coordinate of the river network, achieved by setting

$$\chi = \int_{x_b}^{x} \left(\frac{A_0}{A(x')}\right)^m dx'. \qquad (3)$$

Here, A is the upstream drainage area and A_0 is a reference drainage area used to keep the units of χ in metres. The value of A_0 is set to a value of 1 m^2 so that the values of u^* are comparable to previous studies[40]. We also use a value of 0.45 for m, appropriate for tectonically active regions[41]. Note that if n is not equal to one, the relationship between z and χ is still linear, and linear inverse methods can be used to infer the model parameters. In this way, u^* could be converted to rock uplift rate, provided K and n are known, without changing our ability to reconstruct topography. Therefore, we do not specify a value of n or K to reproduce palaeotopography. If u^* varies in space, we can write a discrete version of equation (2) for pixels in a DEM along a channel,

$$z_i = z_j + (\chi_i - \chi_j) u^* \qquad (4)$$

where the ith pixel is upstream of the jth pixel, and the lowest pixel has an elevation of zero. In the case of the Antarctic Peninsula, the modern topography is expected to be a function of any initial fluvial relief and a component of additional rock uplift. Across the relict part of the landscape, this additional rock uplift corresponds to s.u. Therefore, any point on the relict part of the landscape can be written as:

$$z_i = z_j + (\chi_i - \chi_j) u^* + \text{s.u.}_i \qquad (5)$$

The branching network of river channels and the expectation that u^* varies smoothly in space provides redundant information that enables maps of u^* to be inferred from limited elevation pixels.

Equation 5 shows that similar topographies can be predicted by changing u^* or s.u. However, by forcing the values of u^* or s.u. to vary smoothly across many branches of the river network, the response to changes in these parameters is distinct. For example, the same increase in u^* will lead to a small increase in elevation between nodes that have small differences in χ along the trunk stream, but at confluences, where the change χ is much larger due to the change in upstream drainage area, a larger change in elevation is predicted. By contrast, changes in s.u. will lead to identical increases in elevation regardless of the change in χ. Therefore, linearized inverse schemes enable maps of u^* and s.u. (or maps of surface uplift) to be determined by simplifying the drainage network to reduce the number of nodes, by discretizing space into blocks of constant u^* and s.u. values and by introducing smoothness constraints on u^* and s.u. Therefore, the aim of the inversion is to find a topography that represents the predissected landscape, and this requires finding the model parameters (u^* and s.u. values) that minimize the misfit between predicted and observed elevations of low-relief surfaces.

The expressions for all relict pixels in the dataset can be combined in matrix form as

$$\begin{pmatrix} G \\ \alpha W_u \quad . \\ . \quad \lambda W_{\text{s.u.}} \end{pmatrix} \begin{pmatrix} u^* \\ \text{s.u.} \end{pmatrix} = \begin{pmatrix} z \\ 0 \\ 0 \end{pmatrix}$$

where G is the $2n_{\text{pixel}} \times n_{\text{nodes}}$ containing χ values and entries of one to satisfy equation (5), αW_u ($n_{\text{pixel}} \times n_{\text{pixel}}$) is the weighting matrix for the normalized uplift rate parameters and $\lambda W_{\text{s.u.}}$ ($n_{\text{pixel}} \times n_{\text{pixel}}$) is the weighting matrix for the cumulative surface uplift rate. Importantly, α can control the roughness of both u^* and s.u. and λ can similarly control the roughness of u^* and s.u. (see refs. 27,40 for further details).

With a large value of α, the inversion attempts to minimize the misfit associated with the smoothness constraints (that the Laplacian of the u^* values should be close to zero), resulting in a smooth model. With small values of α, the inversion finds results that fit the data well but are more sensitive to anomalous topography and geomorphic noise, and therefore, results may be meaningless. The same is true for λ and its control on the smoothness of s.u. maps. Within this context, geomorphic noise encapsulates artefacts in the DEM, landslides blocking rivers and over-steepening rivers and small-scale variations in erodibility.

Code Availability

Topographic reconstruction codes are available at https://github.com/adamsmith142/Surface_Uplift.git.

References

40. Fox, M., Carter, A. & Dai, J.-G. How continuous are the "relict" landscapes of southeastern Tibet? *Front. Earth Sci.* **8**, 522 (2020).
41. Kirby, E. & Whipple, K. X. Expression of active tectonics in erosional landscapes. *J. Struct. Geol.* **44**, 54–75 (2012).

Author contributions

All authors contributed to the inception of the study. M.F. and A.C. carried out the topographic analysis and wrote the manuscript. All authors edited the manuscript and contributed to methodological advancement.

Competing interests

The authors declare no competing interests.

Additional information

Supplementary information The online version contains supplementary material available at https://doi.org/10.1038/s41561-023-01336-7.

Correspondence and requests for materials should be addressed to Matthew Fox.

Peer review information *Nature Geoscience* thanks Jane Andersen and the other, anonymous, reviewer(s) for their contribution to the peer review of this work. Primary Handling Editor: James Super, in collaboration with the *Nature Geoscience* team.

Reprints and permissions information is available at www.nature.com/reprints.